Microsystem Technologies (2020) 26:461–473
https://doi.org/10.1007/s00542-019-04542-9

TECHNICAL PAPER

Thermal buckling and forced vibration characteristics of a porous GNP reinforced nanocomposite cylindrical shell

Farzad Ebrahimi[1] · Davoud Hashemabadi[2] · Mostafa Habibi[3] · Hamed Safarpour[1]

Received: 24 April 2019 / Accepted: 6 July 2019 / Published online: 18 July 2019

Abstract
In this research, thermal buckling and forced vibration characteristics of the imperfect composite cylindrical nanoshell reinforced with graphene nanoplatelets (GNP) in thermal environments are presented. Halpin–Tsai nanomechanical model is used to determine the material properties of each layer. The size-dependent effects of GNPRC nanoshell is analyzed using modified couple stress theory. For the first time, in the present study, porous functionally graded multilayer couple stress (FMCS) parameter which changes along the thickness is considered. The novelty of the current study is to consider the effects of porosity, GNPRC, FMCS and thermal environment on the resonance frequencies, thermal buckling and dynamic deflections of a nanoshell using FMCS parameter. The governing equations and boundary conditions are developed using Hamilton's principle and solved by an analytical method. The results show that, porosity, GNP distribution pattern, modified couple stress parameter, length to radius ratio, mode number and the effect of thermal environment have an important role on the resonance frequencies, relative frequency change, thermal buckling, and dynamic deflections of the porous GNPRC cylindrical nanoshell using FMCS parameter. The results of current study can be useful in the field of materials science, micro-electro-mechanical systems and nano electromechanical systems such as microactuators and microsensors.

1 Introduction

According to the recent advantages in nanoscience and technology (Olia et al. 2019; Hosseini et al. 2018), the GNP reinforcement has attracted considerable attention. Recently, Li et al. (2018) studied the effect of GNP on grain size and hardness of GNP/Ni micro/nano composites. Their result showed that the grains of the GNP/Ni composites are finer than pure Ni and the hardness of this composite is higher than the pure Ni, So that they produced micro gear by using the GNP/Ni composite. Rafiee et al. (2009) compared the mechanical properties of epoxy refined by 1% value fraction of the single walled carbon nanotubes (SWNT), multi walled carbon nanotube (DWNT) and GNP with each other. They reported that E, σ_{UTS} and fracture toughness of the composite reinforced by GNPs is higher than other composites. So, GNP is a good alternative for SWCNTs and MWCNTs in many applications. In the field reinforced structures, some researches showed that Habibi et al. (2016, 2017, 2018a, b), Fazaeli et al. (2016), Hosseini et al. (2018), Ghazanfari et al. (2016) and Torabi and Shafieefar (2015) with the aid of some methods the mechanical properties of macro-structures is improved.

Some researches demonstrated that subjoining a very meager value of graphene into the primary polymer matrix can improve mechanical, thermal and electrical properties of the structure (Ebrahimi et al. 2018; Safarpour et al. 2018a, b; Esmailpoor Hajilak et al. 2019; Pourjabari et al. 2019; Habibi et al. 2019; Zehtabiyan-Rezaie et al. 2019; Makki et al. 2019). It is worth mentioning that the nanostructures reinforced by GNP are more applicable in engineering design, so that focus on the dynamic modeling of the nanostructure reinforced by GNP reinforcement is an

✉ Farzad Ebrahimi
febrahimy@eng.ikiu.ac.ir

[1] Department of Mechanics, Faculty of Engineering, Imam Khomeini International University, Qazvin, Iran

[2] Department of Mechanics, Faculty of Engineering, Islamic Azad University of South Tehran Branch, Tehran, Iran

[3] Center of Excellence in Design, Robotics and Automation, School of Mechanical Engineering, Sharif University of Technology, Tehran, Iran

important issue. For this reason, the investigation of the mechanical characteristics of the reinforced strictures have a great importance for engineering design and manufacture. Song et al. (2017) demonstrated the post buckling of the FG reinforced GNPs nanobeams. They indicated that the GNPs have substantial reinforcing effect on the buckling and post buckling of the beams. In another paper, Feng et al. (2017) studied the nonlinear bending of the GNPs reinforced beams. They showed that the high value of GNPs and symmetric distribution in such directions are less susceptible to the nonlinear behavior. According to many researcher's reports, the size effects have a significant role on the mechanical behaviors of the micro/nano structures (Ghadiri et al. 2017; Ghadiri and SafarPour 2017; Mahinzare et al. 2017; Mohammadi et al. 2018). Thus, overlooking these effects may lead to obtain wrong results in designing and manufacturing. It should worth mentioning that classical continuum theory (Shamloofard and Assempour 2019; Shamloofard and Movahhedy 2015) is not validated for modeling any micro/nano structures. Therefore, some methods, such as: molecular dynamic (MD) simulations (Shayan-Amin et al. 2009; Mohammadi et al. 2017, 2018; Tsai and Tu 2010) and non-classical continuum theory are used to study nanostructures. MD simulation includes complicated and time-consuming calculations which are not efficient. In contrast, simple and efficient, higher order continuum mechanic theories, have recently attracted researcher's attentions. As studying the mechanical behaviors of nanoshells relates to submicron dimensions, they could not be correctly predicted by the classical theory. Thus taking into consideration the size effect, higher order continuum theories are used. As an example for size-dependent theories: Ghayesh et al. (2018) demonstrated nonlinear vibration of a FG microplate based on a modified version of the couple stress theory. In their result showed that FG volume fraction, parameters of length-scale, and external force have special effect on the response of the structure. Vibrational behavior of FGM nanobeam based on nonlocal strain gradient elasticity theory (NSGT) is examined by Hadi et al. (2018). Also, they solved those equations with the aid of GDQM. They concluded that, NSGT is the best theory for their problem. Ghayesh and Farajpour (2018) discussed on the nonlinear forced vibration of the nanoscale tubes using NSGT. They developed the equations of the problem by Hamilton's principle. As their interesting results, they showed that, external force has important role on the dynamics behavior. Farokhi and Ghayesh (2018) investigated the effects of DC and AC voltages on the static and dynamic instability of microelectromechanical plate. They employed the modified couple stress theory (MCST) for considering the size effect. Ghayesh (2018) presented the force vibration of the FG viscoelastic microbeams using MCST. In their results, effects of the FG volume fraction, amplitude load and viscoelastic parameters on the forced vibration of the structures are investigated. Khaniki (2018) used Eringen's theory for analyzing of the vibrational behavior of the two-layered nanobeam. The porosity effect on vibrational behavior of the nanotubes based on NSGT is investigated by She et al. (2018). In their work, the effects of temperature variations, porosity and material parameters on the vibrational behavior of the nanotubes are studied. Ke et al. (2012) discussed on the vibration of the FG microbeams with the aid of MCST. In addition, for solving the equations using boundary conditions they used DQM. Shafiei and She (2018) investigated the vibrational characteristics of the FG tubes with the aid of NSGT. They used GDQM for solving the equations. In the results section, they demonstrated the effects of the different boundary condition, material variation, temperature variation, and nonlocal parameter on the vibrational behavior of the structure. Sahmani and Aghdam (2017) studied nonlinear instability of FG-GNPRC nanoshells under hydrostatic pressure using NSGT. Sahmani et al. (2018) investigated the nonlinear vibration of the FG porous GNP micro and nano plates with the aid of NSGT. Barati (2018) studied the forced vibration of the porous plates using NSGT. They showed that, the porosity pattern, nonlocal parameter and the location of the dynamic load have significant effects on the forced vibrational behavior of the nanoplates. Therefore, it is a great significance to study the forced vibration characteristics of a porous GNPRC cylindrical nanoshell using FMCS parameter for the first time.

To the best of our knowledge, no papers have been reported in the literature concerning the forced vibrational behavior of the porous GNPRC nanoshells using FMCS parameter. It is noted that, pervious papers have not considered the effects of porosity, thermal environment, dynamic load, porous GNPRC and size effect on the resonance frequencies and dynamic deflections of the porous GNPRC nanoshell using FMCS parameter and the first order shear deformation (FSDT). The novelty of this paper is considering the porosity, GNPRC, different temperature distributions, size effects and dynamic load implemented on the proposed model based on FSDT. Finally, in the results section show that the GNP distribution patterns, modified couple stress parameter, porosity and thermal environment have important roles on the resonance frequencies, relative frequency changes, and dynamic

deflections of the porous GNPRC cylindrical nanoshell in thermal environments.

2 Multilayer polymer porous composites reinforced GNPs formulations

Here, a cylindrical nanoshell under the dynamic load is modeled. R, h and l are middle surface radius, thickness and length of the cylindrical nanoshell, respectively. Applied dynamic load is shown by q_0 (Fig. 1).

The cylindrical nanoshell is made of composite material. For better grasp of the importance and applications of the current model, Fig. 2 shows a multi-layer GNP/polymer nanocomposite shell. As Fig. 2 displays GNPs are regularly dispersed in each layer of polymer matrix, but in each layer the weight fraction is different from another. Pattern 1 is an isotropic homogeneous plate that GNPs (wt% of GNPs 1%) are regularly distributed, and pattern 2 shows that GNPs weight fraction (wt%) changes since layer to layer along the thickness. As shown in pattern 3 the weight fraction in midplane is the highest and increases layer to layer towards the top layer. In comparison with pattern 2, pattern 3 shows the maximum weight fraction on both top layers, and it decreases to the lowest amount in the mid-plane. Pattern 4 is a non-symmetrical pattern in which weight fraction increments linearly from top to inner surface.

In addition, three different nonuniform patterns for the porous material are shown in Fig. 3.

The volume fraction functions of these four patterns have been represented by

$$\text{Pattern 1:} \quad U-GNPRC: V_{GNP}(k) = V^*_{GNP} \tag{1}$$

$$\text{Pattern 2:} \quad X-GNPRC: V_{GNP}(k) = 2V^*_{GNP}|2k - N_L - 1|/N_L \tag{2}$$

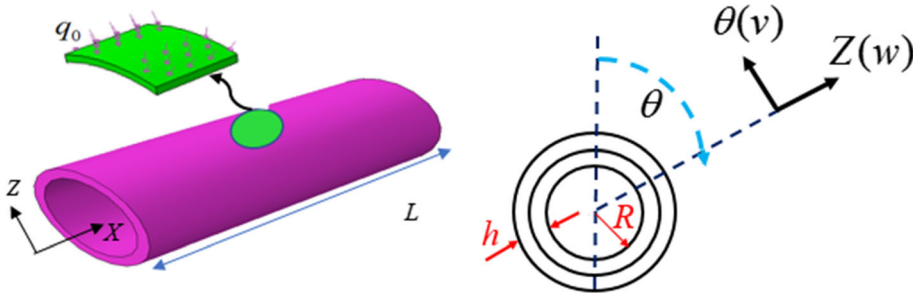

Fig. 1 Geometry of a cylindrical GNPRC nanoshell under dynamic load

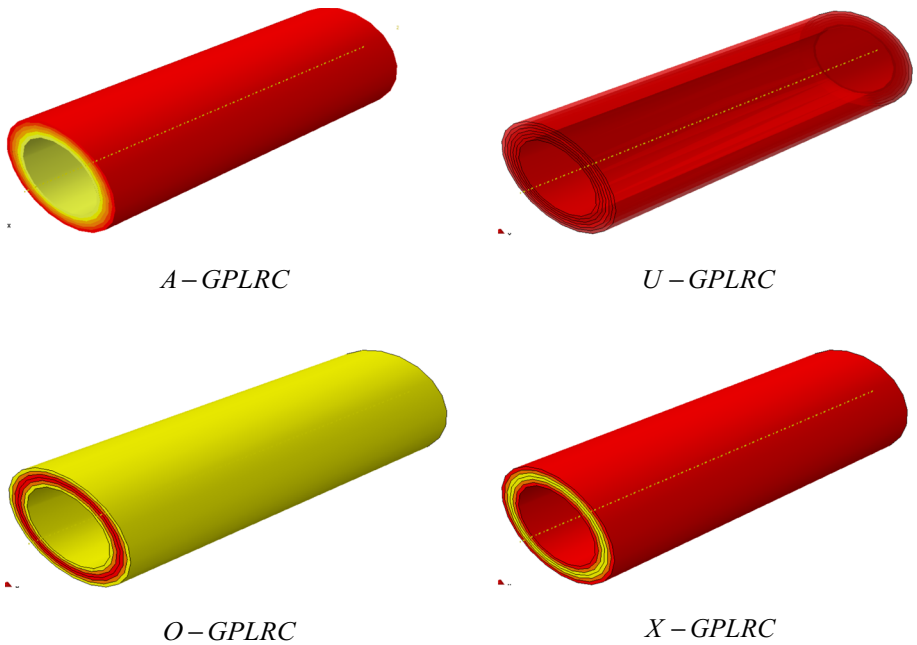

Fig. 2 Different distributions of GNP in GNPRCs cylindrical nanoshell

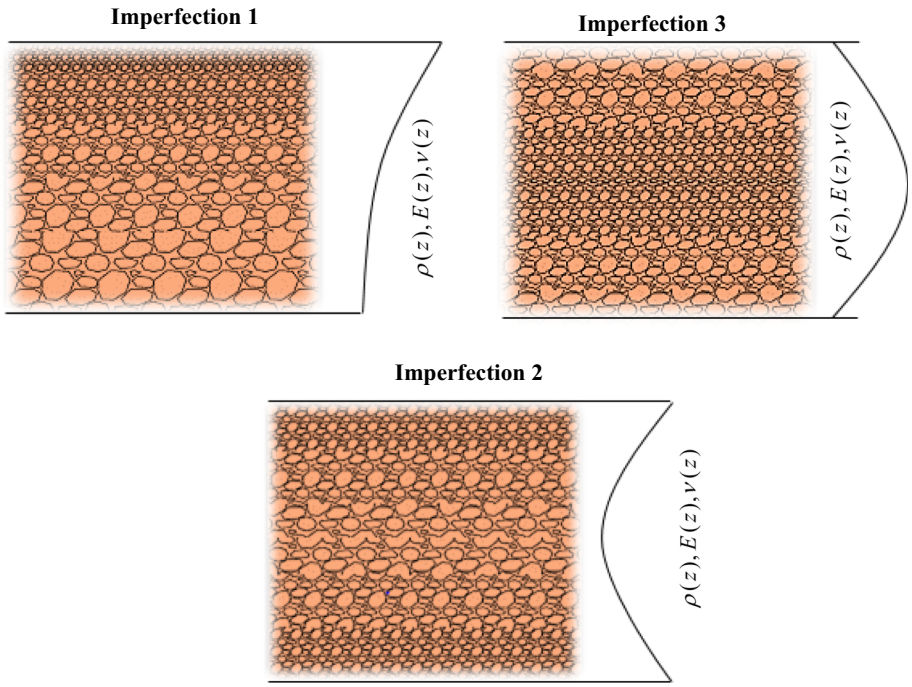

Fig. 3 Schematic representation of the FG porous cylindrical nanoshell with various porosity dispersion

$$\text{Pattern 3:}\quad O-GNPRC: V_{GNP}(k) = 2V^{*}_{GNP}[1-(|2k-N_L-1|/N_L)] \tag{3}$$

$$\text{Pattern 4:}\quad A-GNPRC: V_{GNP}(k) = 2V^{*}_{GNP}(2k-1)/N_L \tag{4}$$

where k is the number of layers of the nanoshell, N_L and V^{*}_{GNP} are total number of layers and GNPs volume fraction. Relation of V^{*}_{GNP} and g_{GNP} can be defined by:

$$V^{*}_{GNP} = \frac{g_{GNP}}{g_{GNP} + (\rho_{GNP}/\rho_m)(1-g_{GNP})} \tag{5}$$

in which, GNPs mass densities and polymer matrix are ρ_{GNP} and ρ_m. Based on Tsai–Halpin model, the elastic modulus of composites reinforced by GNPs approximated by:

$$\begin{aligned} E &= \frac{3}{8}E_L + \frac{5}{8}E_T, \\ E_L &= \frac{1+\xi_L n_L V_{GPL}}{1-n_L V_{GPL}}E_m, \quad E_T = \frac{1+\xi_T n_T V_{GPL}}{1-n_T V_{GPL}}E_m \end{aligned} \tag{6}$$

where E is the effective modulus of composites reinforced by GNPs. In addition, for unidirectional lamina, E_L and E_T are longitudinal and transverse moduli. In Eq. (6) the GNP geometry factors (ξ_L and ξ_T) and other parameters are given by:

$$\begin{aligned} \xi_L &= 2(\mathbb{Z}_{GNP}/h_{GNP}), \quad \xi_t = 2(b_{GNP}/h_{GNP}), \\ n_L &= \frac{(E_{GNP}/E_M)-1}{(E_{GNP}/E_M)+\xi_L}, \quad n_T = \frac{(E_{GNP}/E_M)-1}{(E_{GNP}/E_M)+\xi_T} \end{aligned} \tag{7}$$

where $\mathbb{Z}_{GNP}$, h_{GNP}, R_{GNP} are the average length, thickness and radius of the GNPs. By using rule of mixture, young's module ($\bar{E}$), Mass density ($\bar{\rho}$), Poisson's ratio ($\bar{\nu}$), and thermal expansion ($\bar{\alpha}$) of the GNP/polymer composite are expressed as:

$$\begin{aligned} \bar{E} &= E_{GNP}V_{GNP} + E_M V_M, \\ \bar{\rho} &= \rho_{GNP}V_{GNP} + \rho_M V_M, \\ \bar{\nu} &= \nu_{GNP}V_{GNP} + \nu_M V_M, \\ \bar{\alpha} &= \alpha_{GNP}V_{GNP} + \alpha_M V_M. \end{aligned} \tag{8}$$

The mechanical properties of the porous GNPRC cylindrical shell are presented by (Sahmani et al. 2018):

$$\begin{aligned} E_{eff} &= \bar{E}[1-\Gamma_P S(z)], \\ \rho_{eff} &= \bar{\rho}[1-\Gamma_m S(z)], \\ \alpha_{eff} &= \bar{\alpha}[1-\Gamma_p S(z)], \\ \nu_{eff} &= 0.221\left(1-\frac{\rho_{eff}}{\bar{\rho}}\right) \\ &\quad + \bar{\nu}\left[1+0.342\left(1-\frac{\rho_{eff}}{\bar{\rho}}\right)^2 - 1.21\left(1-\frac{\rho_{eff}}{\bar{\rho}}\right)\right] \end{aligned} \tag{9}$$

where

$$S(z)=\begin{cases}\cos\left(\frac{\pi z}{2h}+\frac{\pi}{4}\right) & for\ imperfection\ 1\\ \cos\left(\frac{\pi z}{h}\right) & for\ imperfection\ 2\\ 1-\cos\left(\frac{\pi z}{h}\right) & for\ imperfection\ 3\end{cases}$$
$$\Gamma_m=1.121\left[1+(-1+\Gamma_p S(z))^{1/2.3}\right]/S(z) \tag{10}$$

In Eqs. (9) and (10) Γ_p and Γ_m are porosity and density coefficients, respectively.

2.1 Mathematical modeling

According to the Taylor's series expansion, displacement components are as below (Ebrahimi et al. 2019; Safarpour et al. 2019):

$$\begin{aligned}u(x,\theta,z,t)&=u_0(x,\theta,t)+zu_1(x,\theta,t)\\ v(x,\theta,z,t)&=(1+z/R)v_0(x,\theta,t)+zv_1(x,\theta,t)\\ w(x,\theta,z,t)&=w_0(x,\theta,t)\end{aligned} \tag{11}$$

Here, $u_0(x,\theta,t)$, $v_0(x,\theta,t)$ and $w_0(x,\theta,t)$ indicate the displacements of the neutral surface along x, θ and z directions respectively. Also, $u_1(x,\theta,t)$ and $v_1(x,\theta,t)$ represent the rotations of a cross section around θ and x-directions. In addition, the three-dimensional stress–strain relation can be expressed as follows:

$$\begin{bmatrix}\sigma_{xx}\\ \sigma_{\theta\theta}\\ \sigma_{zz}\\ \sigma_{x\theta}\\ \sigma_{xz}\\ \sigma_{\theta z}\end{bmatrix}=\begin{bmatrix}\bar{Q}_{11}&\bar{Q}_{12}&\bar{Q}_{13}&0&0&0\\ \bar{Q}_{12}&\bar{Q}_{22}&\bar{Q}_{23}&0&0&0\\ \bar{Q}_{13}&\bar{Q}_{23}&\bar{Q}_{33}&0&0&0\\ 0&0&0&\bar{Q}_{44}&0&0\\ 0&0&0&0&\bar{Q}_{55}&0\\ 0&0&0&0&0&\bar{Q}_{66}\end{bmatrix}\begin{bmatrix}\varepsilon_{xx}-\alpha_1\Delta T\\ \varepsilon_{\theta\theta}-\alpha_2\Delta T\\ \varepsilon_{zz}-\alpha_3\Delta T\\ \varepsilon_{x\theta}\\ \varepsilon_{xz}\\ \varepsilon_{\theta z}\end{bmatrix} \tag{12}$$

In Eq. (12) thermal expansion and temperature changes are α and ΔT, respectively. The minimum potential energy for motion and boundary conditions equations states that:

$$\int_{t_1}^{t_2}(\delta T-\delta U+\delta W_1-\delta W_2)dt=0 \tag{13}$$

The strain energy (Zahabi et al. 2018) of the nanoshell is:

$$U=\frac{1}{2}\iiint_V(\sigma_{ij}\varepsilon_{ij}+m_{ij}^s\chi_{ij}^s)R\,dx d\theta dz \tag{14}$$

In Eq. (14), strain and stress components are ε_{ij} and σ_{ij}, which are presented by Barooti et al. (2017). In addition, m_{ij} and χ_{ij}^s are the components of the symmetric rotation and higher order stress tensor, which can be expressed as:

$$\begin{aligned}\chi_{ij}^s&=\frac{1}{2}(\varphi_{i,j}+\varphi_{j,i})\\ m_{ij}^s&=2l^2\mu\chi_{ij}^s\end{aligned} \tag{15}$$

where $\emptyset_i$ and l represent the extremely small rotation vector and FMCS parameter is symmetric rotation, and can be shown as below:

$$l=l_{GNP}V_{GNP}+l_MV_M \tag{16}$$

Moreover, the kinetic energy of the GNPRC cylindrical nanoshell considering FMCS parameter can be obtained as:

$$T=\frac{1}{2}\int_Z\iint_A\rho\left\{\dot{u}^2+\dot{v}^2+\dot{w}^2\right\}R\,dz\,dx\,d\theta \tag{17}$$

For a typical isotropic cylindrical shell which is in exposure to high temperature environment, it is assumed that the temperature distributed across its thickness. Hence, work done of temperature change can be obtained as:

$$W_1=\frac{1}{2}\iint_A\left[N_1^T\left(\frac{\partial w_0}{\partial x}\right)^2+N_2^T\left(\frac{\partial v_0}{\partial x}\right)^2\right]R\,dx\,d\theta \tag{18}$$

where thermal resultants are N_1^T and N_2^T. Both of them can be obtained as:

$$\begin{aligned}N_1^T&=\int_{-h/2}^{h/2}(\bar{Q}_{11}+\bar{Q}_{12}+\bar{Q}_{13})\,\alpha(T-T_0)dz,\\ N_2^T&=\int_{-h/2}^{h/2}(\bar{Q}_{21}+\bar{Q}_{22}+\bar{Q}_{23})\,\alpha(T-T_0)dz.\end{aligned} \tag{19}$$

Coefficients of thermal expansion are presented as:

$$\alpha=[\alpha_{xxe}\ \ \alpha_{\theta\theta e}\ \ \alpha_{zze}\ \ 0\ \ 0\ \ 0]^T \tag{20}$$

Temperature changes linearly along the thickness from T_m (at the outer surface) to T_c (at the inner surface) is supposed. The work done of applied forces obtained as:

$$W_2=\frac{1}{2}\left\{q_{dynamic}w^2\right\}R\,dV \tag{21}$$

In which, $q_{dynamic}$ is applied dynamic load. Substituting Eqs. (14), (17), (18) and (21) into Eq. (13) the motion equations of the porous GNP cylindrical nanoshell in thermal environment can be obtained as follows:

$$
\begin{aligned}
&\left[\frac{\partial N_{xx}}{\partial x}+\frac{1}{R}\frac{\partial N_{x\theta}}{\partial \theta}+\frac{1}{2R^2}\left(-\frac{\partial Y_{\theta\theta}}{\partial \theta}+\frac{\partial Y_{zz}}{\partial \theta}\right)+\frac{1}{2R}\frac{\partial^2 Y_{zx}}{\partial \theta\,\partial x}+\frac{1}{2R^2}\frac{\partial^2 Y_{\theta z}}{\partial \theta^2}\right]\delta u\\
&\quad+\left[\frac{\partial N_{x\theta}}{\partial x}+\frac{1}{R}\frac{\partial}{\partial \theta}N_{\theta\theta}+\frac{Q_{z\theta}}{R}+\frac{1}{2}\right.\\
&\quad\left.\left\{\frac{1}{R}\frac{\partial}{\partial x}(-Y_{xx}+Y_{\theta\theta})-\frac{1}{R^2}\frac{\partial Y_{\theta x}}{\partial \theta}-\frac{\partial^2 Y_{xz}}{\partial x^2}-\frac{Y_{xz}}{R^2}-\frac{1}{R}\frac{\partial^2 Y_{z\theta}}{\partial \theta\,\partial x}\right\}\right]\delta v\\
&\quad-N_2^T\frac{\partial^2 v}{\partial x^2}\delta v\\
&\quad+\left[\frac{\partial Q_{xz}}{\partial x}+\frac{1}{R}\frac{\partial Q_{z\theta}}{\partial \theta}-\frac{N_{\theta\theta}}{R}-\frac{1}{2R^2}\frac{\partial^2 Y_{\theta x}}{\partial \theta^2}-\frac{1}{2R^2}\frac{\partial Y_{zx}}{\partial \theta}+\frac{1}{2R}\frac{\partial Y_{\theta z}}{\partial x}+\frac{\partial^2 Y_{x\theta}}{2\partial x^2}\right]\delta w_0\\
&\quad+\left[-\frac{1}{2R}\frac{\partial^2}{\partial \theta\,\partial x}(Y_{xx}-Y_{\theta\theta})-N_1^T\frac{\partial^2 w}{\partial x^2}\right]\delta w\\
&\quad+\left[\frac{\partial M_{xx}}{\partial x}+\frac{1}{R}\frac{\partial M_{\theta\theta}}{\partial \theta}-Q_{xz}+\frac{1}{2}\frac{\partial Y_{\theta x}}{\partial x}-\frac{1}{2R}\frac{\partial}{\partial \theta}(Y_{zz}-Y_{\theta\theta})\right]\delta u_1\\
&\quad+\left[\frac{Y_{zz}}{R}+\frac{1}{2R}\frac{\partial^2 T_{zx}}{\partial \theta\,\partial x}+\frac{1}{2R^2}\frac{\partial^2 T_{\theta z}}{\partial \theta^2}\right]\delta u_1\\
&\quad+\left[\frac{1}{R}\frac{\partial M_{\theta\theta}}{\partial \theta}+\frac{\partial M_{x\theta}}{\partial x}-Q_{z\theta}+\frac{1}{2}\frac{\partial}{\partial x}\left(Y_{zz}-Y_{xx}+\frac{T_{\theta\theta}}{R}\right)\right]\delta v_1\\
&\quad+\left[-\frac{1}{2}\frac{\partial Y_{\theta x}}{\partial \theta}+\frac{Y_{xz}}{2R}-\frac{1}{2R}\frac{\partial^2 T_{\theta z}}{\partial \theta\,\partial x}-\frac{1}{2}\frac{\partial^2 T_{zx}}{\partial x^2}\right]\delta v_1\\
&=\left\{I_0\frac{\partial^2 u}{\partial t^2}+I_1\frac{\partial^2 \psi_x}{\partial t^2}\right\}\delta u+\left\{I_0\frac{\partial^2 v}{\partial t^2}+I_1\frac{\partial^2 \psi_\theta}{\partial t^2}\right\}\delta v\\
&\quad+I_0\frac{\partial^2 w}{\partial t^2}\delta w_0+\left\{I_1\frac{\partial^2 u}{\partial t^2}+I_2\frac{\partial^2 \psi_x}{\partial t^2}\right\}\delta u_1\\
&\quad+\left\{I_1\frac{\partial^2 v}{\partial t^2}+I_2\frac{\partial^2 \psi_\theta}{\partial t^2}\right\}\delta v_1+q_{dynamic}\delta w
\end{aligned}
\tag{22}
$$

where parameters used in Eq. (22) are presented as:

$$
\begin{aligned}
&(N_{xx},N_{\theta\theta},N_{x\theta})=\int_{-h/2}^{h/2}(\sigma_{xx},\sigma_{\theta\theta},\sigma_{x\theta})dz,\\
&(M_{xx},M_{\theta\theta},M_{x\theta})=\int_{-h/2}^{h/2}(\sigma_{xx},\sigma_{\theta\theta},\sigma_{x\theta})zdz,\\
&(Q_{xz},Q_{z\theta})=\int_{-h/2}^{h/2}k_s(\sigma_{xz},\sigma_{z\theta})dz,\\
&(Y_{xx},Y_{\theta\theta},Y_{zz},Y_{x\theta},Y_{xz},Y_{z\theta})\\
&=\int_{-h/2}^{h/2}(m_{xx},m_{\theta\theta},m_{zz},m_{x\theta},m_{xz},m_{z\theta})dz,\\
&(T_{xx},T_{\theta\theta},T_{zz},T_{x\theta},T_{xz},T_{z\theta})\\
&=\int_{-h/2}^{h/2}(m_{xx},m_{\theta\theta},m_{zz},m_{x\theta},m_{xz},m_{z\theta})zdz.
\end{aligned}
\tag{23}
$$

2.2 Solution procedure

In this section, analytical method is implemented to solve the governing equations of MSGT-based on GPLRC nanoshell. In addition, in this research, the proposed model is simply supported in $x = 0$, L and $\theta = \pi/2$, $3\pi/2$. Thus, the displacement fields can be calculated as:

$$
\begin{Bmatrix}
u_0(x,\theta,t)\\ v_0(x,\theta,t)\\ w_0(x,\theta,t)\\ u_1(x,\theta,t)\\ v_1(x,\theta,t)
\end{Bmatrix}
=\sum_{m=1}^{\infty}\sum_{n=1}^{\infty}
\begin{Bmatrix}
U_{0mn}\cos\left(\frac{m\pi}{L}x\right)\cos(n\theta)\\
V_{0mn}\sin\left(\frac{m\pi}{L}x\right)\sin(n\theta)\\
W_{0mn}\sin\left(\frac{m\pi}{L}x\right)\cos(n\theta)\\
U_{1mn}\cos\left(\frac{m\pi}{L}x\right)\cos(n\theta)\\
V_{1mn}\sin\left(\frac{m\pi}{L}x\right)\sin(n\theta)
\end{Bmatrix}\sin(\omega t)
\tag{24}
$$

where $\{U_{0mn}, V_{0mn}, W_{0mn}, \Psi_{xmn}, \Psi_{\theta mn}\}$ are the unknown Fourier coefficients that need to be determined for each n and m values. Also, n and m are the circumferential and axial wave numbers, respectively. For vibration analysis of the structure, by substituting Eq. (24) into Eq. (22), one obtains:

$$
\left(\begin{bmatrix}
k_{1,1} & k_{1,2} & k_{1,3} & k_{1,4} & k_{1,5}\\
k_{2,1} & k_{2,2} & k_{2,3} & k_{2,4} & k_{2,5}\\
k_{3,1} & k_{3,2} & k_{3,3} & k_{3,4} & k_{3,5}\\
k_{4,1} & k_{4,2} & k_{4,3} & k_{4,4} & k_{4,5}\\
k_{5,1} & k_{5,2} & k_{5,3} & k_{5,4} & k_{5,5}
\end{bmatrix}
-\omega_{ex}^2\begin{bmatrix}
m_{1,1} & m_{1,2} & m_{1,3} & m_{1,4} & m_{1,5}\\
m_{2,1} & m_{2,2} & m_{2,3} & m_{2,4} & m_{2,5}\\
m_{3,1} & m_{3,2} & m_{3,3} & m_{3,4} & m_{3,5}\\
m_{4,1} & m_{4,2} & m_{4,3} & m_{4,4} & m_{4,5}\\
m_{5,1} & m_{5,2} & m_{5,3} & m_{5,4} & m_{5,5}
\end{bmatrix}\right)
\begin{Bmatrix}U_0\\V_0\\W_0\\\psi_x\\\psi_\theta\end{Bmatrix}
=\begin{bmatrix}0\\0\\q_{dynamic}\\0\\0\end{bmatrix}
\begin{Bmatrix}U_0\\V_0\\W_0\\\psi_x\\\psi_\theta\end{Bmatrix}
\tag{25}
$$

In which, ω_{ex} is the excitation frequency and applied dynamic load ($q_{dynamic}$) is defined as:

$$
q_{dynamic}=\sum_{m=1}^{\infty}\sum_{n=1}^{\infty}q_0\sin\left(\frac{m\pi}{L}x\right)\cos(n\theta)\sin(\omega t),
\tag{26}
$$

Solution of Eq. (26) gives the dynamic deflection and excitation frequency of the porous FG-GPLRC cylindrical nanoshell. The dimensionless excitation frequency and forced vibration amplitude are defined as:

$$\Omega = 10 \times \omega_{ex} L\sqrt{\rho/E}, \quad \bar{W}_{uniform} = W_{0mn}\frac{10Eh^3}{L^4 q_0}. \qquad (27)$$

3 Results and discussion

In the result section, a porous GNP cylindrical nanoshell in thermal environment is modeled with the simply supported boundary conditions. After modeling the current structure, the effects of the porosity, patterns of GNP distribution, FMCS parameter, radius to length ratio, mode number and thermal environment on resonance frequencies and dynamic deflections are studied in detail. Generally, the first part of our result is validation of the model with the aid of previous papers in literature. In the second part, effects of porosity and some various parameters on resonance frequencies and dynamic deflections of the porous GNP nanoshell in thermal environments are investigated.

3.1 Model validation

According to Fig. 3, in these value of length scale parameter ($l = R/3$), MCST has a better agreement with the results of MD simulation which is reported by Ansari et al. (2012). So, considering the three value of length scale parameter ($l = R/3$) is a good suggestion for dynamic analysis of a nanoshell using MCST (Fig. 4).

Table 1 presents a comparison study between obtained natural frequencies of simply supported nanoshells with considering FMCS parameter from current study and previous papers. High agreement between the dimensionless natural frequency of current study and those of Tadi Beni et al. (2016) is shown.

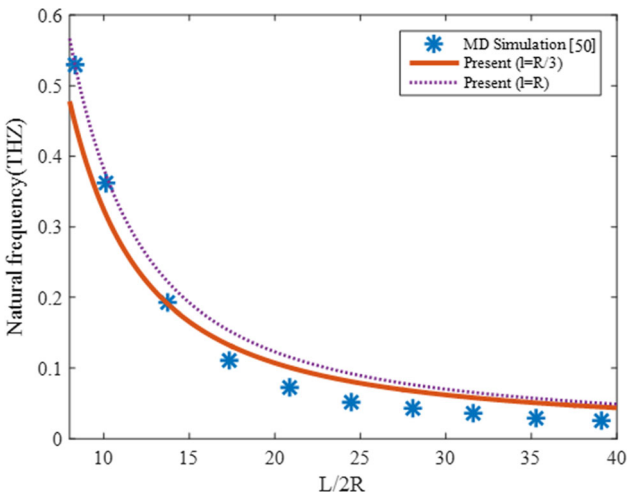

Fig. 4 Comparison of the natural frequency of cylindrical nanoshell with the results obtained by MD simulation (Ansari et al. 2012)

As another verification, Table 2 compares the results for dimensionless natural frequency of the cylindrical shell with different GNP distribution patterns with the reported results with those obtained by Liu et al. (2018).

3.2 Parametric results

In this section the analytical results are presented for a simply supported porous GNP cylindrical nanoshell using FMCS parameter in thermal environment. The model is a cylindrical shell with the total thickness of h_{GNP} = 1.5 nm, length of a_{GNP} = 2.5 μm and radius of R_{GNP} = 0.75 μm. Table 3 gives the mechanical properties of GNP. The property parameters of epoxy are assumed to be temperature-dependent. In the following sections the effects of different parameters on the excitation frequency, dimensionless amplitude and relative frequency changes of the structure are investigated.

Temperature dependency of the porous materials are defined as follows:

$$\alpha_m = \frac{45(0.0005\Delta T + 1)}{10^6 \times K} \text{ and } E = (-3.52 + 0.0034T)\ \text{GPa, in which } T = \Delta T + T_0.$$

3.3 The effects of different parameter on excitation frequency and dimensionless amplitude

The effect of weight function on dynamic deflection and resonance frequency of the GNPRC cylindrical nanoshell is shown in Fig. 5. In this figures, different values of weight function (g_{GPL}) are examined. It is evident that dynamic deflection of the GNPRC cylindrical nanoshell is affected by the magnitude of excitation frequency of dynamic load. In fact, dynamic deflection increases smoothly with the increase of excitation frequency. At a certain value of excitation frequency, a considerable increase is observed in deflection of GNPRC cylindrical nanoshell. The reason is that the excitation frequency of dynamic load coincides with the natural frequency of the GNPRC cylindrical nanoshell which leads to the resonance phenomena. It is seen that resonance frequency of the GNPRC cylindrical nanoshell decreases by decreasing the weight function. This is because of an increase in the weight function which leads to an increase in the stiffness of structure, and causes resonance frequency and stability to increase.

The effects of different GPL distribution patterns on the dynamic deflection and resonance frequency of the GPLRC cylindrical nanoshell is illustrated in Fig. 6. It can be seen that as GPL distribution patterns increases from 1 to 4, the resonance frequency increases, this leads to an increase in the instability of structure. In other words, pattern 4 gives

Table 1 Dimensionless natural frequencies of isotropic homogeneous nanoshells

h/R	*n*	Tadi Beni et al. (2016) (l = 0)	Present (l = 0)	Tadi Beni et al. (2016) (l = h)	Present study (l = h)
0.02	1	0.1954	0.19536215	0.1955	0.19543206
	2	0.2532	0.25271274	0.2575	0.25731258
	3	0.2772	0.27580092	0.3067	0.30621690
0.05	1	0.1959	0.19542305	0.1963	0.19585782
	2	0.2623	0.25884786	0.2869	0.28543902
	3	0.3220	0.31407326	0.4586	0.45457555

Table 2 dimensionless natural frequency of GNPRC nanoshells

$m\pi L/l_{GPL}$	Epoxy Liu et al. (2018)	Epoxy present	GNP-UD Liu et al. (2018)	GNP-UD present	GNP-A Liu et al. (2018)	GNP-A present
2	0.9659	0.9365985	2.3674	2.303659	2.2517	2.242659
5	2.6997	2.6698544	6.6185	6.486598	5.4878	5.463265
10	5.6503	5.6265987	13.8540	13.80756	9.6421	9.635698

Table 3 Epoxy and GNP properties (Wu et al. 2017)

Material properties	Epoxy	GNP
Young's modulus (GPa)	3	1010
Density (kg m^{-3})	1200	1062.5
Poisson's ratio	0.34	0.186
Thermal expansion coefficient(10^{-6}/K)	60	5

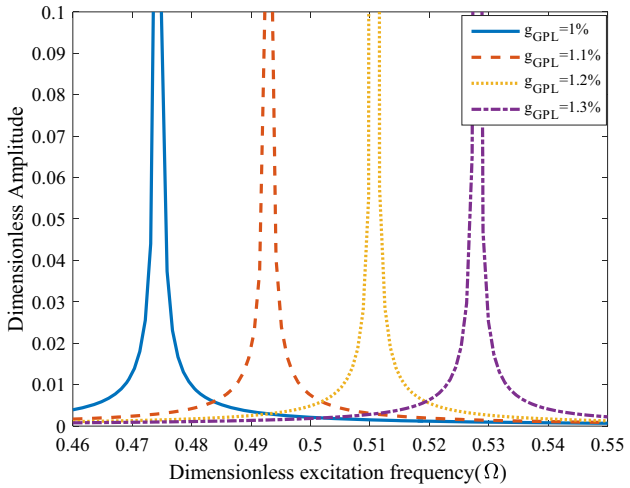

Fig. 5 Resonance frequency and dynamic deflection of the cylindrical nanoshell for different weight fraction ($\Delta T = 20K$, l = R/3, Pattern 2, L/R = 10, R/h = 10 and n = m = 1)

larger resonance frequencies than other patterns. This behavior stems from the mathematical function which was presented in previous section. It is worth mentioning that,

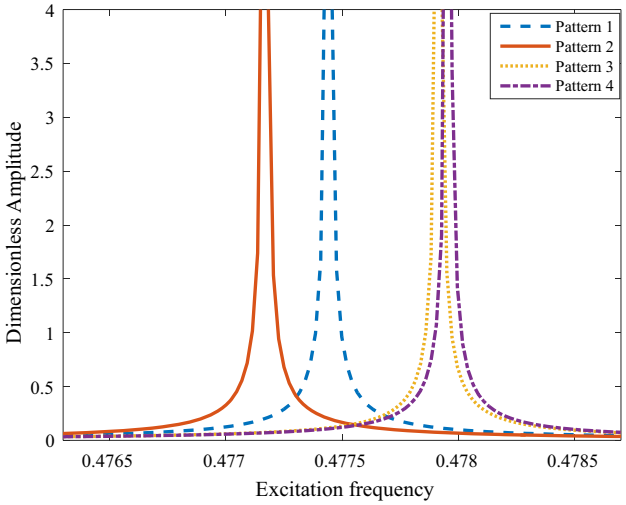

Fig. 6 Resonance frequency and dynamic deflection of the cylindrical nanoshell for different GNP distribution patterns ($\Delta T = 20K$, l = R/3, L/R = 10, R/h = 10 and n = m = 1)

the resonance frequency of the structure in patterns 3 and 4 are close to each other.

In Fig. 7, the effect of FMCS parameter on the excitation frequency and dynamic deflection of the porous GNP cylindrical nanoshell is studied for X-GNPRC pattern. As an important result, the FMCS parameters have a remarkable effect on the resonance frequencies of the structure. An increase in the FMCS parameters leads to increase the resonance frequency so that this matter can cause an improvement in the stability of the porous GNP cylindrical.

The effects of R/h and temperature changes on resonance frequency of the porous GNP cylindrical nanoshell

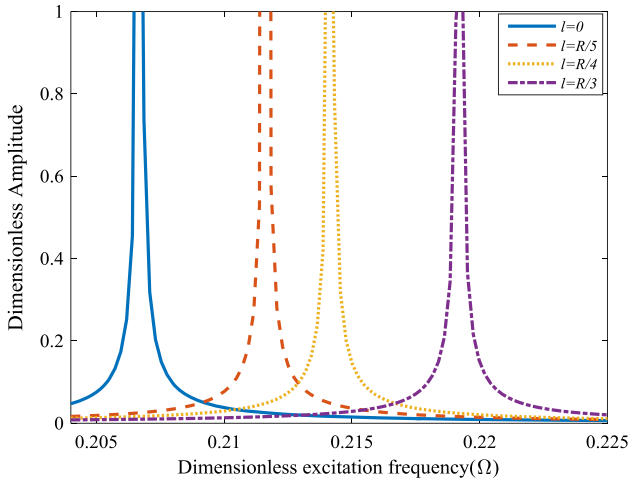

Fig. 7 Resonance frequency and dynamic deflection of the cylindrical nanoshell for different modified couple stress parameter ($\Delta T = 20K$, Pattern 2, L/R = 10, R/h = 10 and n = m = 1)

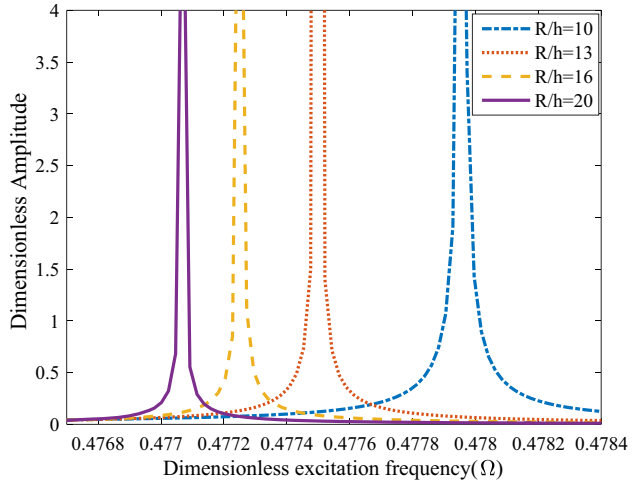

Fig. 8 Resonance frequency and dynamic deflection of the cylindrical nanoshell for different radius to thickness ratios ($\Delta T = 0K$, l = R/3, Pattern 4, L/R = 10 and n = m = 1)

are presented in Figs. 8 and 9. Based on Fig. 8, by increasing the R/h, the resonance frequency and stability decline. In addition, Fig. 8 indicates that an increase in the temperature changes cause to increase in the resonance frequency, and leads to decline the stability of structure.

3.4 Different parameters effects on relative frequency change

The percentage value in parentheses denotes the relative frequency increase $(\omega_C - \omega_M)$, where ω_C and ω_M are natural frequencies with and without GPL, respectively. Figure 10 show the relative frequency changes of the FG-GPLRC cylindrical nanoshell with different total number of layers (N_L). As expected, the fundamental frequencies of

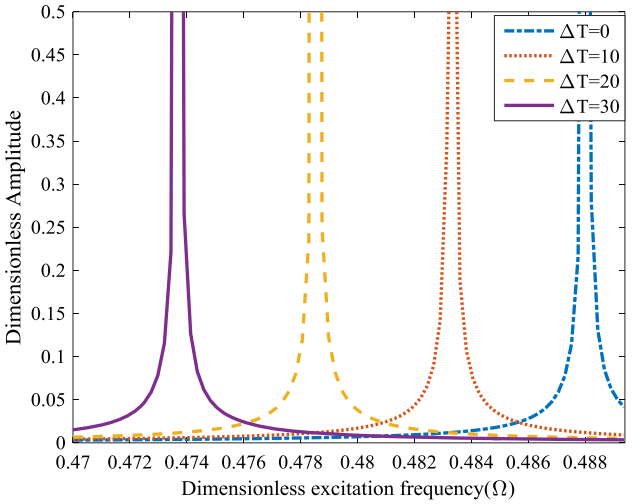

Fig. 9 Resonance frequency and dynamic deflection of the cylindrical nanoshell for different temperature changes (l = R/3, Pattern 4, L/R = 10, R/h = 10 and n = m = 1)

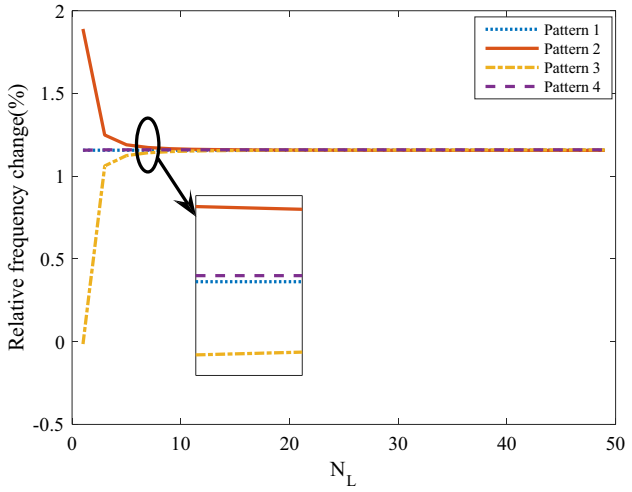

Fig. 10 The effect of N_L on the relative frequency change for different patterns of GNP/epoxy ($\Delta T = 10K$, l = R/3, Pattern 2, L/R = 10, R/h = 10 and n = m = 1)

the structure with GPL distribution pattern 1 are not affected by N_L since they are homogeneous. For the cylindrical nanoshells with pattern 2 in which GPLs are non-uniformly dispersed, their fundamental frequencies decrease with increasing the total number of layers to N_L = 7, then they remain almost unchanged when N_L is further increased. In contrast, this trend is reversed for GPL distribution pattern 3. Among the three non-uniform patterns considered, the fundamental frequency of the structure with GPL pattern 1 is least affected by the change in N_L. As a good suggestion, the multilayer shell is modeled in the current study. According to Fig. 10 by increasing the number of layers ($1 < N_L < 7$) the natural frequency and stability of the nanostructure change (for non-uniform GPL

distribution patterns 2 and 3). It is observed that, in the non-uniform GPL distribution pattern 3, by increasing of the number of layers, the natural frequency and stability of the nanostructure increase. Also, for the other uniform and non-uniform distribution patterns, number of layers of the GPL is not important. The other amazing result is that, by increasing the number of layers in the non-uniform GPL distribution pattern 2, the natural frequency and stability decrease.

Figures 11 and 12 show the effects of FMCS parameters and temperature changes on the relative frequency of the porous GNPRC cylindrical nanoshell, respectively. Based on Fig. 10, an increase in the material length parameter leads to an increase in the natural frequency and a decrease in the stability of the structure. At a certain value of temperature change, a considerable increase is observed in deflection of GNPRC cylindrical nanoshell. The reason of this trend is that the buckling phenomena occurs in this temperature. According to Fig. 12, by increasing the FMCS parameters, an enhancement for relative frequency of the structure is observed. The amazing result is that; mode number has any effect on the relative frequency changes of the porous GNP cylindrical nanoshell. By increasing the weight fraction, the structure becomes softer, so that it is a reason for increasing the relative frequency changes.

Figures 13, 14 and 15 illustrate the effect of porosity coefficient, and temperature changes on natural frequency (THz) for different porosity distributions using non-classical continuum theory. According to figures, by decreasing the temperature changes, stability and natural frequency of the nanoshell see a decrease. The figure shows that an increase in porosity coefficient increases the natural

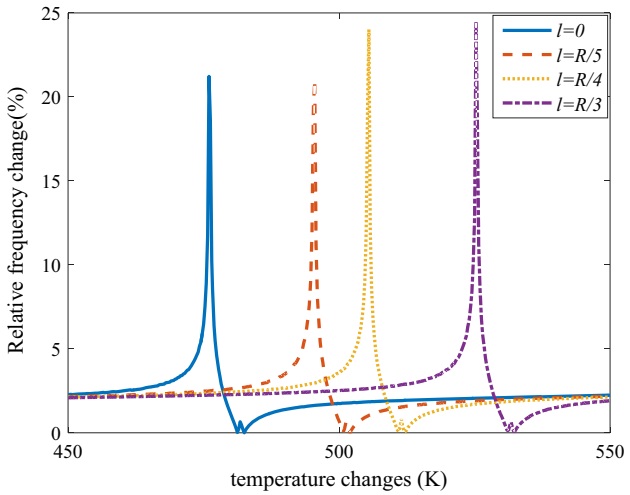

Fig. 11 The effect of the temperature changes on the relative frequency change for different FMCS parameter (Pattern 2, L/R = 10, R/h = 10 and n = m = 1)

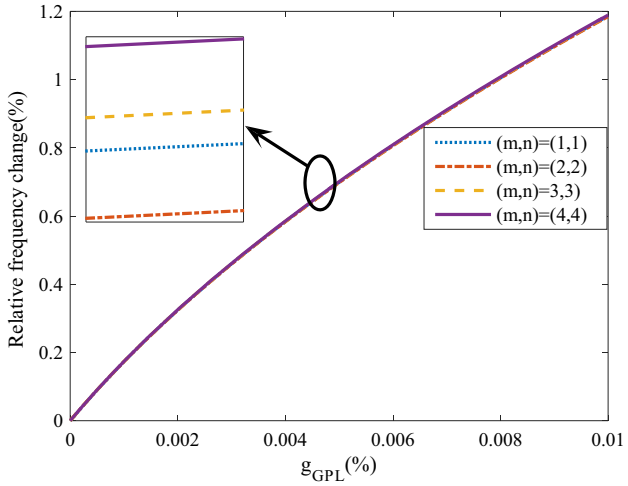

Fig. 12 The effect of weight fraction on the relative frequency change for different mode numbers ($\Delta T = 10K$, l = R/3, Pattern 2, L/R = 10, R/h = 10)

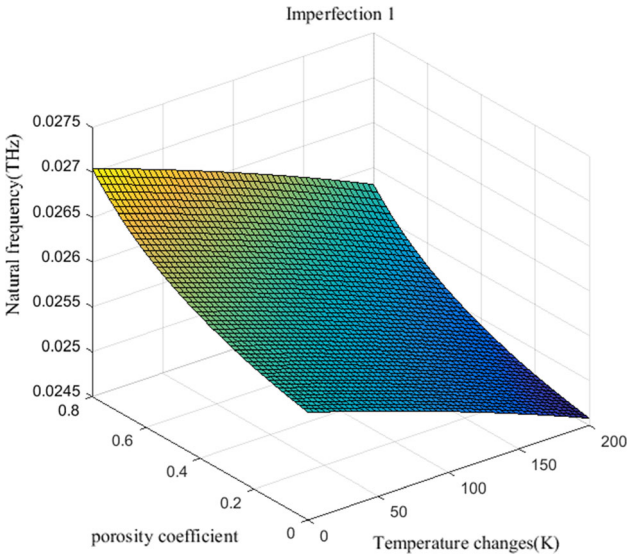

Fig. 13 The effects of temperature changes and porosity coefficient on the natural frequency (THz) of the simply supported porous GNPRC nanoshell with considering imperfection 1

frequency and causes an increase in stability of nanostructure. The difference between Figs. 13, 14 and 15 is that, by increasing the porosity coefficient in porosity distribution 1, the natural frequency increases in the form of nonlinear changes. Porosity distribution 2 has similar trend as can be seen in Fig. 14, but by increasing the porosity coefficient in porosity distribution 3, the natural frequency increases in the form of linear changes.

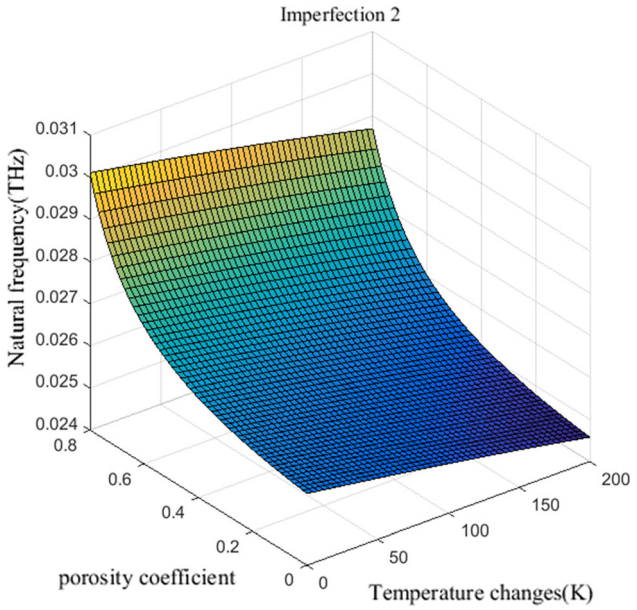

Fig. 14 The effects of temperature changes and porosity coefficient on the natural frequency (THz) of the simply supported porous GNPRC nanoshell with considering imperfection 2

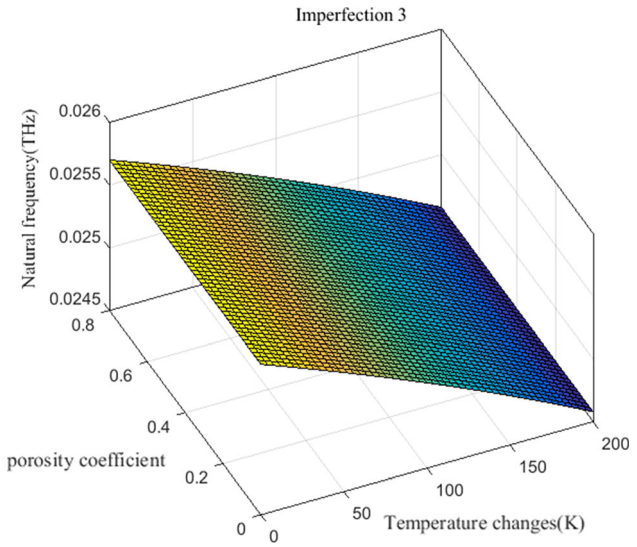

Fig. 15 The effects of temperature changes and porosity coefficient on the natural frequency (THz) of the simply supported porous GNPRC nanoshell with considering imperfection 3

4 Conclusions

In this article, size-dependent thermal buckling, forced and free vibrational characteristics of a porous composite cylindrical nanoshell reinforced by GNPs in thermal environment are presented. The size-dependent porous GNP nanoshell is analyzed using FMCS parameter. At the first time, in this article, FMCS constant which changes along the thickness direction is considered. With the aid of the Hamilton's principle, the motion equations and non-classic boundary conditions are obtained. Excellent agreements are observed with comparison the results of this research and those of others and MD simulation which confirmed the accuracy and validity of this continuum mechanic model. The influences of some key parameters such as, GNP distribution patterns, FMCS parameter, length to radius ratio, mode number, and thermal environment on the resonance frequencies, relative frequency change and dynamic deflections are studied. The main results of this article are presented as below:

1. It is observed that the resonance frequency increases as the FMSC parameter and weight fraction increase, and it decreases as the temperature difference increases.
2. The results show that A-GNP pattern presents larger resonance frequency than other patterns.
3. An increase in the temperature change causes to increase in the relative frequency which decreases the stability of the structure, however this trend is reversed for weight fraction of GNP.
4. By increasing R/h parameter, the resonance frequency and stability of the porous GNP cylindrical nanoshell tends to increase.
5. By increasing the porosity coefficient in imperfection 1, the natural frequency increases as nonlinear changes and the imperfection 2 has a similar trend with imperfection 1, but effect of porosity coefficient on natural frequency in imperfection 3 is linear.

References

Ansari R, Gholami R, Rouhi H (2012) Vibration analysis of single-walled carbon nanotubes using different gradient elasticity theories. Compos B Eng 43:2985–2989

Barati MR (2018) A general nonlocal stress–strain gradient theory for forced vibration analysis of heterogeneous porous nanoplates. Eur J Mech A Solids 67:215–230

Barooti MM, Safarpour H, Ghadiri M (2017) Critical speed and free vibration analysis of spinning 3D single-walled carbon nanotubes resting on elastic foundations. Eur Phys J Plus 132:6

Ebrahimi F, Habibi M, Safarpour H (2018) On modeling of wave propagation in a thermally affected GNP-reinforced imperfect nanocomposite shell. Eng Comput. https://doi.org/10.1007/s00366-018-0669-4

Ebrahimi F, Hajilak ZE, Habibi M, Safarpour H (2019) Buckling and vibration characteristics of a carbon nanotube-reinforced spinning cantilever cylindrical 3D shell conveying viscous fluid flow and carrying spring-mass systems under various temperature distributions. Proc Inst Mech Eng Part C J Mech Eng Sci. https://doi.org/10.1177/0954406219832323

Esmailpoor Hajilak Z, Pourghader J, Hashemabadi D, Sharifi Bagh F, Habibi M, Safarpour H (2019) Multilayer GPLRC composite cylindrical nanoshell using modified strain gradient theory. Mech Based Design Struct Mach 14:1–25. https://doi.org/10.1080/15397734.2019.1566743

Farokhi H, Ghayesh MH (2018) Nonlinear mechanics of electrically actuated microplates. Int J Eng Sci 123:197–213
Fazaeli A, Habibi M, Ekrami AA (2016) Experimental and finite element comparison of mechanical properties and formability of dual phase steel and ferrite–pearlite steel with the same chemical composition. Metall Eng 19:84–93
Feng C, Kitipornchai S, Yang J (2017) Nonlinear bending of polymer nanocomposite beams reinforced with non-uniformly distributed graphene platelets (GPLs). Compos B Eng 110:132–140
Ghadiri M, SafarPour H (2017) Free vibration analysis of size-dependent functionally graded porous cylindrical microshells in thermal environment. J Thermal Stress 40(1):55–71. https://doi.org/10.1080/01495739.2016.1229145
Ghadiri M, Shafiei N, Safarpour H (2017) Influence of surface effects on vibration behavior of a rotary functionally graded nanobeam based on Eringen's nonlocal elasticity. Microsyst Technol 23:1045–1065. https://doi.org/10.1007/s00542-016-2822-6
Ghayesh MH (2018) Dynamics of functionally graded viscoelastic microbeams. Int J Eng Sci 124:115–131
Ghayesh MH, Farajpour A (2018) Nonlinear mechanics of nanoscale tubes via nonlocal strain gradient theory. Int J Eng Sci 129:84–95
Ghayesh MH, Farokhi H, Gholipour A, Tavallaeinejad M (2018) Nonlinear oscillations of functionally graded microplates. Int J Eng Sci 122:56–72
Ghazanfari A, Assempuor A, Habibi M, Hashemi R (2016) Investigation on the effective range of the through thickness shear stress on forming limit diagram using a modified Marciniak–Kuczynski model. Modares Mech Eng 16:137–143
Habibi M, Hashemi R, Sadeghi E, Fazaeli A, Ghazanfari A, Lashini H (2016) Enhancing the mechanical properties and formability of low carbon steel with dual-phase microstructures. J Mater Eng Perform 25:382–389
Habibi M, Ghazanfari A, Assempour A, Naghdabadi R, Hashemi R (2017) Determination of forming limit diagram using two modified finite element models. Mech Eng. https://doi.org/10.22060/MEJ.2016.664
Habibi M, Hashemi R, Tafti MF, Assempour A (2018a) Experimental investigation of mechanical properties, formability and forming limit diagrams for tailor-welded blanks produced by friction stir welding. J Manuf Process 31:310–323
Habibi M, Hashemi R, Ghazanfari A, Naghdabadi R, Assempour A (2018b) Forming limit diagrams by including the M–K model in finite element simulation considering the effect of bending. Proc Inst Mech Eng Part L J Mater Des Appl 232:625–636
Habibi M, Mohammadgholiha M, Safarpour H (2019) Wave propagation characteristics of the electrically GNP-reinforced nanocomposite cylindrical shell. J Braz Soc Mech Sci Eng 41:221
Hadi A, Nejad MZ, Hosseini M (2018) Vibrations of three-dimensionally graded nanobeams. Int J Eng Sci 128:12–23
Hosseini M, Bahaadini R, Makkiabadi M (2018a) Application of the Green function method to flow-thermoelastic forced vibration analysis of viscoelastic carbon nanotubes. Microfluid Nanofluid 22:6
Hosseini S, Habibi M, Assempour A (2018b) Experimental and numerical determination of forming limit diagram of steel-copper two-layer sheet considering the interface between the layers. Modares Mech Eng 18:174–181
Ke L-L, Wang Y-S, Yang J, Kitipornchai S (2012) Nonlinear free vibration of size-dependent functionally graded microbeams. Int J Eng Sci 50:256–267
Khaniki HB (2018) On vibrations of nanobeam systems. Int J Eng Sci 124:85–103
Li M, Liu J, Zhang X, Tian Y, Jiang K (2018) Fabrication of graphene/nickel composite microcomponents using electroforming. Int J Adv Manuf Technol 96:3191–3196
Liu D, Kitipornchai S, Chen W, Yang J (2018) Three-dimensional buckling and free vibration analyses of initially stressed functionally graded graphene reinforced composite cylindrical shell. Compos Struct 189:560–569
Mahinzare M, Mohammadi K, Ghadiri M, Rajabpour A (2017) Size-dependent effects on critical flow velocity of a SWCNT conveying viscous fluid based on nonlocal strain gradient cylindrical shell model. Microfluid Nanofluid 21:123
Makki M, Izadi AI, Jalili B (2019) Numerical analysis of a multi-stage evacuation desalination in Tehran city. Water Energy Int 61:53–57
Mohammadi K, Mahinzare M, Rajabpour A, Ghadiri M (2017) Comparison of modeling a conical nanotube resting on the Winkler elastic foundation based on the modified couple stress theory and molecular dynamics simulation. Eur Phys J Plus 132:115
Mohammadi K, Mahinzare M, Ghorbani K, Ghadiri M (2018a) Cylindrical functionally graded shell model based on the first order shear deformation nonlocal strain gradient elasticity theory. Microsyst Technol 24:1133–1146
Mohammadi K, Rajabpour A, Ghadiri M (2018b) Calibration of nonlocal strain gradient shell model for vibration analysis of a CNT conveying viscous fluid using molecular dynamics simulation. Comput Mater Sci 148:104–115
Olia H, Torabi M, Bahiraei M, Ahmadi MH, Goodarzi M, Safaei MR (2019) Application of nanofluids in thermal performance enhancement of parabolic trough solar collector: state-of-the-art. Appl Sci 9:463
Pourjabari A, Hajilak ZE, Mohammadi A, Habibi M, Safarpour H (2019) Effect of porosity on free and forced vibration characteristics of the GPL reinforcement composite nanostructures. Comput Math Appl 77(10):2608–2626. https://doi.org/10.1016/j.camwa.2018.12.041
Rafiee MA, Rafiee J, Wang Z, Song H, Yu Z-Z, Koratkar N (2009) Enhanced mechanical properties of nanocomposites at low graphene content. ACS Nano 3:3884–3890
Safarpour H, Hajilak ZE, Habibi M (2018a) A size-dependent exact theory for thermal buckling, free and forced vibration analysis of temperature dependent FG multilayer GPLRC composite nanostructures restring on elastic foundation. Int J Mech Mater Design. https://doi.org/10.1007/s10999-018-9431-8
Safarpour H, Ghanizadeh SA, Habibi M (2018b) Wave propagation characteristics of a cylindrical laminated composite nanoshell in thermal environment based on the nonlocal strain gradient theory. Eur Phys J Plus 133:532
Safarpour H, Pourghader J, Habibi M (2019) Influence of spring-mass systems on frequency behavior and critical voltage of a high-speed rotating cantilever cylindrical three-dimensional shell coupled with piezoelectric actuator. J Vib Control 25(9):1543–1557. https://doi.org/10.1177/1077546319828465
Sahmani S, Aghdam M (2017) A nonlocal strain gradient hyperbolic shear deformable shell model for radial postbuckling analysis of functionally graded multilayer GPLRC nanoshells. Compos Struct 178:97–109
Sahmani S, Aghdam MM, Rabczuk T (2018) Nonlocal strain gradient plate model for nonlinear large-amplitude vibrations of functionally graded porous micro/nano-plates reinforced with GPLs. Compos Struct 198:51–62
Shafiei N, She G-L (2018) On vibration of functionally graded nanotubes in the thermal environment. Int J Eng Sci 133:84–98
Shamloofard M, Assempour A (2019) Development of an inverse isogeometric methodology and its application in sheet metal forming process. Appl Math Model 73:266–284

Shamloofard M, Movahhedy MR (2015) Development of thermo-elastic tapered and spherical superelements. Appl Math Comput 265:380–399

Shayan-Amin S, Dalir H, Farshidianfar A (2009) Molecular dynamics simulation of double-walled carbon nanotube vibrations: comparison with continuum elastic theories. J Mech 25:337–343

She G-L, Ren Y-R, Yuan F-G, Xiao W-S (2018) On vibrations of porous nanotubes. Int J Eng Sci 125:23–35

Song M, Kitipornchai S, Yang J (2017) Free and forced vibrations of functionally graded polymer composite plates reinforced with graphene nanoplatelets. Compos Struct 159:579–588

Tadi Beni Y, Mehralian F, Zeighampour H (2016) The modified couple stress functionally graded cylindrical thin shell formulation. Mech Adv Mater Struct 23:791–801

Torabi MA, Shafieefar M (2015) An experimental investigation on the stability of foundation of composite vertical breakwaters. J Mar Sci Appl 14:175–182

Tsai J-L, Tu J-F (2010) Characterizing mechanical properties of graphite using molecular dynamics simulation. Mater Des 31:194–199

Wu H, Kitipornchai S, Yang J (2017) Thermal buckling and postbuckling of functionally graded graphene nanocomposite plates. Mater Des 132:430–441

Zahabi H, Torabi M, Alamatian E, Bahiraei M, Goodarzi M (2018) Effects of geometry and hydraulic characteristics of shallow reservoirs on sediment entrapment. Water 10:1725

Zehtabiyan-Rezaie N, Alvandifar N, Saffaraval F, Makkiabadi M, Rahmati N, Saffar-Avval M (2019) A solar-powered solution for water shortage problem in arid and semi-arid regions in coastal countries. Sustain Energy Technol Assess 35:1–11